Proper Scaling of the Anomalous Hall Effect

Yuan Tian, Li Ye, and Xiaofeng Jin*

Surface Physics Laboratory and Physics Department, Fudan University, Shanghai 200433, China

(Received 30 March 2009; published 21 August 2009)

Working with epitaxial films of Fe, we succeeded in independent control of different scattering processes in the anomalous Hall effect. The result clearly exposed the fundamental flaws of the conventional scaling $\rho_{AH} = f(\rho_{xx})$ between the anomalous Hall resistivity and longitudinal resistivity. A new scaling $\rho_{AH} = f(\rho_{xx0}, \rho_{xx})$ that also involves the residual resistivity has been established which helps identify the intrinsic and extrinsic mechanisms of the anomalous Hall effect.

DOI: 10.1103/PhysRevLett.103.087206 PACS numbers: 75.47.Np, 72.15.Eb, 73.50.Jt

While the ordinary Hall effect has been well understood as a result of the Lorentz force deflecting the charge carriers, the mechanism of the anomalous Hall effect (AHE) [1] has remained controversial despite the long history of research, because its rich phenomenology defies the standard classification methodology, prompting conflicting reports claiming the dominance of various processes [2–13].

Experimentally, a unified scaling describing the AHE resistivity ρ_{AH} in terms of the longitudinal resistivity ρ_{xx} is still missing, while four different types of $\rho_{AH} = f(\rho_{xx})$ were claimed in various materials: (a) $b\rho_{xx}^2$ (e.g., Fe) [14–17], (b) $a\rho_{xx}$ (e.g., ultrapure Ni at low temperature) [18], (c) $a\rho_{xx} + b\rho_{xx}^2$ (e.g., Co) [19,20], and (d) $b\rho_{xx}^\alpha$ (e.g., Ni) with $1 < \alpha < 2$ [21]. Theoretically, Karplus and Luttinger first proposed that the spin-orbit interaction together with the interband mixing resulted in an intrinsic anomalous velocity in the direction transverse to the electric field [2], which gave $\rho_{int} \propto \rho_{xx}^2$. However, Smit suggested that the extrinsic skew scattering at impurities was responsible for the AHE, which gave $\rho_{sk} \propto \rho_{xx}$ [3]. Berger further proposed that the extrinsic side jump at impurities could account for the $\rho_{sj} \propto \rho_{xx}^2$ relation [5]. In contrast, the Karplus-Luttinger mechanism was recently revived in the language of Berry phase [10–12], and it was thought again to play the dominant role in the AHE [19,22–24]; meanwhile, a real space Berry phase theory was also developed to account for the AHE [13]. Despite the controversies, it is generally accepted that the total anomalous Hall conductivity (σ_{AH}) consists of three terms: $\sigma_{AH} = \sigma_{int} + \sigma_{sk} + \sigma_{sj}$, where σ_{int} is the intrinsic Karplus-Luttinger term, σ_{sk} is the extrinsic skew scattering, and σ_{sj} the generalized extrinsic side jump [9,25]. It has been a great experimental challenge to separate the intrinsic from extrinsic contributions.

In this work we have developed a new experimental strategy that goes beyond the existing paradigms. Usually the longitudinal resistivity is taken as a quantity characteristic only of the material, so traditionally besides temperature, ρ_{xx} was varied only by changing the impurity concentration of the material. However, such an approach has the deficiency that it could modify not only the extrinsic but also the intrinsic contributions in the AHE, often complicating the interpretation of the experimental results. Instead, we are tuning the resistivity ρ_{xx} by varying the thickness of Fe film, an idea similar to the control of the coefficient of viscosity for fluid in thin tube by varying its diameter. It is this novel approach that leads to the true scaling of the AHE, by which we develop a strategy that can possibly separate out the intrinsic from extrinsic contributions.

Fe films of thickness ranging from 1.5 to 93 nm were epitaxially grown on undoped GaAs(001) at 300 K by molecular beam epitaxy with its orientations relative to the substrate, Fe[001] ‖ GaAs[001] and Fe[100] ‖ GaAs[100], then capped with a 4 nm thick MgO to prevent oxidation in air; the experimental details were described elsewhere [26,27]. The films were patterned into the form of a standard Hall bar along [110] with the magnetic field along [001]. The transport measurements were carried out in a physical property measurement system (Quantum Design PPMS-9T system). The magnetoresistance in Fe films at 5 T is smaller than 0.5%, and the magnetization in Fe films thicker than 1 nm reaches its bulk value and changes little within the temperature range of 5–320 K. Figure 1(a) shows several representative sets of ρ_{xy} vs H curves measured between 5 and 320 K for a 6.5 nm thick Fe film. $\rho_{AH}(T)$ is then obtained as the zero field extrapolation of the high field data as shown in the figure, and is displayed in Fig. 1(b). $\rho_{xx}(T)$ was measured simultaneously and is shown in Fig. 1(c). From Figs. 1(b) and 1(c), the ρ_{AH} versus ρ_{xx} curve for the 6.5 nm Fe film can be deduced and is displayed in Fig. 1(d), together with representative data for other thicknesses varying between 1.5 and 93 nm.

The set of data in Fig. 1(d) provides an opportunity to unveil the phonon contribution to the AHE—a long-standing controversial issue [3,6,28]. Following the observation in bulk Fe reported in Refs. [14,15], we used $b\rho_{xx}^2$ to fit the data in Fig. 1(d), but found a significant deviation from the dashed lines as the Fe films were thinner than 6.5 nm. This means that other terms must be considered in Fe thin films although they may be neglected in the bulk.

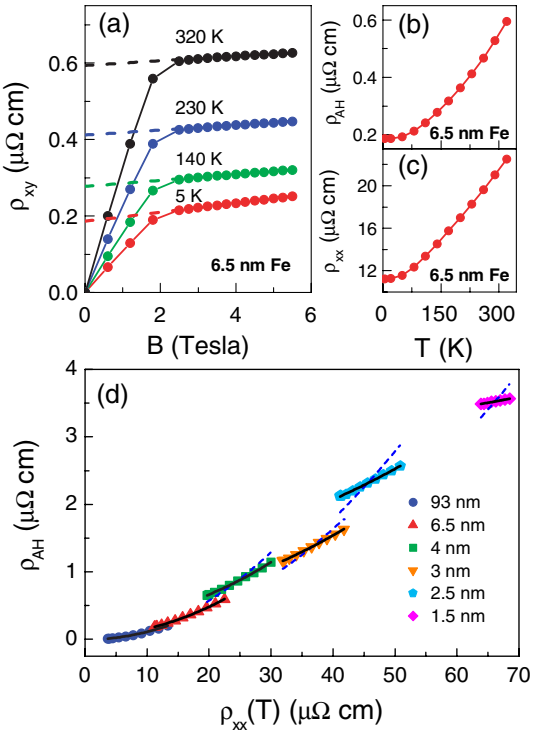

FIG. 1 (color online). (a) ρ_{xy} vs B curves for 6.5 nm film. (b), (c) ρ_{AH} and ρ_{xx} as functions of temperature for 6.5 nm film, respectively. (d) ρ_{AH} and ρ_{xx} for various film thicknesses. The dashed blue line and the solid black line are fitting results with $\rho_{\mathrm{AH}} = b'\rho_{xx}^2$ and $\rho_{\mathrm{AH}} = a'\rho_{xx0} + b\rho_{xx}^2$, respectively.

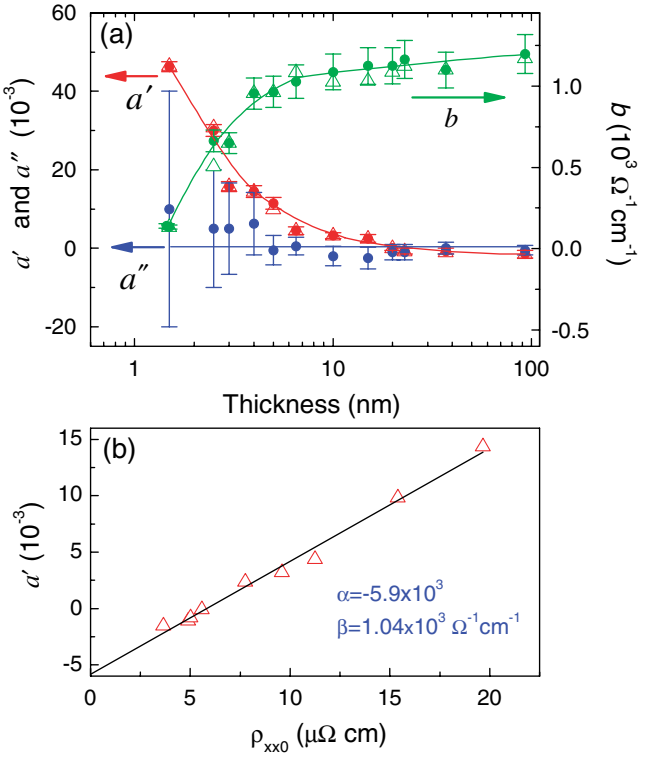

FIG. 2 (color online). (a) Solid red, blue, and green dots represent the parameters a', a'', and b (marked by the arrows), respectively; red and green triangles are the set of a' and b after taking $a'' = 0$. Solid curves are guide to the eye. (b) Red triangles are a' (after taking $a'' = 0$) versus ρ_{xx0} for films above 4 nm. Black line is the linear description by $a' = \alpha + \beta\rho_{xx0}$.

To include the role of the skew scattering, a linear term $\rho_{\mathrm{sk}} = a\rho_{xx}$ is conventionally introduced [17,19,20,24], which implies $\rho_{\mathrm{sk}} = a\rho_{xx0} + a\rho_{xxT}$ according to the Matthiessen rule, where ρ_{xx0} and ρ_{xxT} are the residual and phonon-induced resistivity, respectively. Thus the contributions to ρ_{AH} from phonons and defects are treated on the equal footings, which is not justified. Theoretically it was already pointed out that phonons should have a much smaller effect on skew scattering [28]. To clarify this, we first treat them as two independent sources, i.e., $\rho_{\mathrm{sk}} = a'\rho_{xx0} + a''\rho_{xxT}$, then determine the values of a' and a'' by fitting $\rho_{\mathrm{AH}} = a'\rho_{xx0} + a''\rho_{xxT} + b\rho_{xx}^2$ to the data in Fig. 1(d) using the experimentally measured ρ_{AH}, ρ_{xx0}, ρ_{xxT}, and ρ_{xx} for different film thicknesses. The fitting parameters of a', a'', and b coming out from the best fits are presented in Fig. 2(a), from which it is evident that a' and a'' are indeed distinctly different, and $a'' \approx 0$. After putting $a'' = 0$, we show in black solid lines in Fig. 1(d) the good fittings by $\rho_{\mathrm{AH}} = a'\rho_{xx0} + b\rho_{xx}^2$, and in Fig. 2(a) the corresponding new set of a' and b. The fact that $a'' = 0$ is the first experimental evidence that phonon contribution to the skew scattering in the anomalous Hall resistivity is negligibly small. In addition, as noted in Fig. 2(a), a' is actually not a constant but exhibits strong thickness or ρ_{xx0} dependence. This dependence is further analyzed in Fig. 2(b) and can be described by a simple function of $a' = \alpha + \beta\rho_{xx0}$, where α and β are real constants. It should be mentioned here that in this Letter we focus our attention only on films thicker than 4 nm where $b \approx 1.1 \times 10^3\ \Omega^{-1}\,\mathrm{cm}^{-1}$ is almost constant; the results in the ultrathin regime where b is decreasing deserve a separate discussion elsewhere.

To demonstrate the superiority of the new scaling ($\rho_{\mathrm{AH}} = a'\rho_{xx0} + b\rho_{xx}^2$) over the commonly held old one ($\rho_{\mathrm{AH}} = a_{\mathrm{sk}}\rho_{xx} + b\rho_{xx}^2$) [17,19,20,24], we compare them side by side in Fig. 3, using the same set of experimental raw data without involving any complicated data fitting. Accordingly, a linear relationship would be expected from $\rho_{\mathrm{AH}}/\rho_{xx}$ vs ρ_{xx} for the old scaling [Figs. 3(a)–3(c)], but ρ_{AH} vs ρ_{xx}^2 for the new one [Figs. 3(d)–3(f)], respectively. The comparisons show unambiguously that the new scaling works much better, especially in the thin limit where the old scaling deviates the most. It becomes clear now that a proper scaling for the AHE should involve not only ρ_{xx} but also ρ_{xx0}, i.e., $\rho_{\mathrm{AH}} = f(\rho_{xx0}, \rho_{xx})$—an important fact that has long been hidden. With experimental tuning of the film thickness, we have discovered an empirical relation for the AHE in Fe:

$$\rho_{\mathrm{AH}} = (\alpha\rho_{xx0} + \beta\rho_{xx0}^2) + b\rho_{xx}^2 \qquad (1)$$

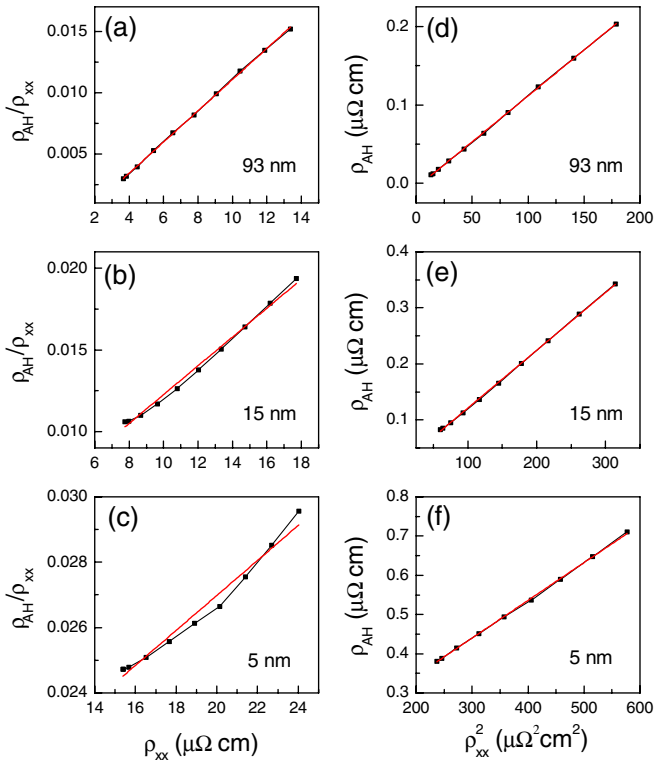

FIG. 3 (color online). Black squares are experimental raw data. The gray (red) lines are linear plots for (a)–(c) ρ_{AH}/ρ_{xx} vs ρ_{xx} and (d)–(f) ρ_{AH} vs ρ_{xx}^2.

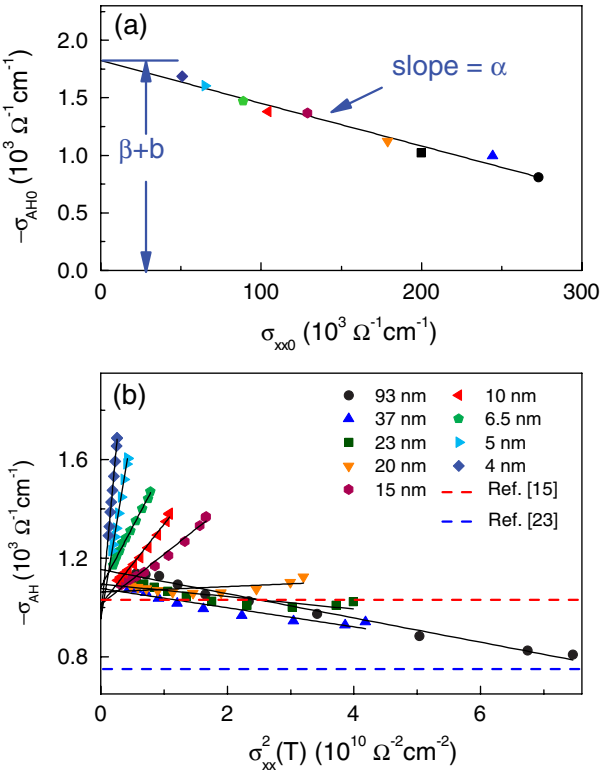

FIG. 4 (color online). (a) $-\sigma_{AH0}$ vs σ_{xx0} measured at 5 K, where colors and shapes are the same as in (b). Black line is the linear description by $-\sigma_{AH0} = \alpha\sigma_{xx0} + (\beta + b)$ (b) $-\sigma_{AH}$ vs σ_{xx}^2 for various film thicknesses. The black lines are description by Eq. (2) for various film thicknesses. The red (upper) dashed line and the blue (lower) dashed line correspond to the $-\sigma_{AH}$ values measured from iron whisker [15] and calculated from the Berry curvature [23], respectively.

$$\sigma_{AH} = -(\alpha\sigma_{xx0}^{-1} + \beta\sigma_{xx0}^{-2})\sigma_{xx}^2 - b, \qquad (2)$$

where $\sigma_{xx0} = 1/\rho_{xx0}$ is the residual conductivity, while ρ_{AH} and σ_{AH} are related by $\rho_{AH} = -\sigma_{AH}\rho_{xx}^2$ in the limit $\rho_{AH} \ll \rho_{xx}$ [well justified as seen in Fig. 1(b) and 1(c)]. Next we attempt to determine more accurately all the relevant parameters α, β, and b without resorting to fitting (Fig. 2). Figure 4(a) presents a plot of $-\sigma_{AH0}$ (residual anomalous Hall conductivity) versus σ_{xx0}, as shown by the dots, using the experimental raw data measured at 5 K for different film thicknesses. At 5 K, both σ_{AH} and σ_{xx} reach their residual values, so we have $\sigma_{AH} \approx \sigma_{AH0}$ and $\sigma_{xx} \approx \sigma_{xx0}$, then Eq. (2) becomes $\sigma_{AH0} = -\alpha\sigma_{xx0} - (\beta + b)$; the experimental data can be well described by this equation using the black line in the figure, and the corresponding constants are extracted as $\alpha = -3.7 \times 10^{-3}$, $(\beta + b) = 1.8 \times 10^3\ \Omega^{-1}\,\mathrm{cm}^{-1}$; therefore, $\beta = 0.7 \times 10^3\ \Omega^{-1}\,\mathrm{cm}^{-1}$.

To gain further insight into the physical meaning of the new scaling, we wish to relate it to the various microscopic mechanisms of AHE. Up to now, theoretical interpretation of the scaling of the AHE has been based on a weak scattering expansion in which only a single scattering mechanism dominates both the transverse and longitudinal resistivities [25]. Such studies seem to show that the intrinsic Karplus-Luttinger and extrinsic side-jump contributions are inseparable because the latter are independent of the strength and density of the scatters. In the low (high) temperature limit where phonon (impurity) scattering is irrelevant, it is true that the side jump (β) appears together with the intrinsic contribution (b), as seen in Fig. 4(a) at 5 K. However, in a mixed regime where both phonon and impurity scatterings contribute, if the impurity scattering dominates in the transverse resistivity over the phonon contribution even though it is negligible in the longitudinal resistivity, it is then possible to separate out the intrinsic Karplus-Luttinger (b term) from the side-jump (β term) as well as the skew-scattering (α term) contributions.

We plot the experimental raw data in Fig. 4(b) according to Eq. (2), in which each curve corresponds to a specific film thickness with the temperature ranging from 5 to 290 K. As σ_{xx}^2 goes to zero, the anomalous Hall conductivity σ_{AH} for various film thicknesses with different residual resistivity converges nicely to a common value $b \approx 1.1 \times 10^3\ \Omega^{-1}\,\mathrm{cm}^{-1}$ that is almost identical to the b value in $\rho_{AH} = b\rho_{xx}^2$ obtained from bulk Fe whisker measured at room temperature [15], as marked by the upper (red) dashed line. This nontrivial universality must reflect the intrinsic nature of the material in the b term in Eq. (1),

which was verified to come mostly from the Karplus-Luttinger intrinsic contribution [23]. On the other hand, the $\alpha\rho_{xx0}$ term in Eq. (1) is only the conventional extrinsic skew scattering.

However, the interpretation of the $\beta\rho_{xx0}^2$ term in Eq. (1) is less obvious. One possibility is that it comes from the second-order contribution of the extrinsic skew scattering as predicted in [28]. Yet its magnitude compared to the first-order term ($\beta\rho_{xx0}^2/\alpha\rho_{xx0} \approx 0.7$–$3.7$ for films with $4 < d < 93$ nm) is much too large for the weak-scattering limit, arguing unfavorably although not completely ruling out this possibility. The fact that the $\beta\sigma_{xx0}^{-2}\sigma_{xx}^2$ term in Eq. (2) behaves the same as the skew scattering as a function of temperature (via σ_{xx}^2) implies that the former is also a kind of impurity originated term. Unfortunately the calculation of impurity and phonon contributions to the side jump remains a big theoretical challenge [25], thereby preventing us from making a definite conclusion about their relative strengths. However, the new scaling revealed by the present experiment suggests that this β term is presumably the long sought after extrinsic side jump if the phonon contribution to the side jump is not relevant; this finding should stimulate further theoretical investigations on the role of phonons in the AHE. Within this scenario it becomes clear in Fig. 4(b) that σ_{AH} is increasingly dominated by the intrinsic Karplus-Luttinger mechanism as other extrinsic processes decay progressively, i.e., $\sigma_{\mathrm{AH}} = (\sigma_{\mathrm{int}} + \sigma_{\mathrm{sk}} + \sigma_{\mathrm{sj}}) \rightarrow \sigma_{\mathrm{int}}$ as $\sigma_{xx}^2 \rightarrow 0$. This corresponds to a process in which the extrinsic terms ($\sigma_{\mathrm{sk}} + \sigma_{\mathrm{sj}}$) attributed to the impurity scattering ought to be washed out, thereby shrinking to zero; in the meantime, the intrinsic one σ_{int}, which originated from the electronic band structure of the material, should be the only robust one that is known to be less sensitive to the temperature.

It should be pointed out that although a simple $\rho_{\mathrm{AH}} = b\rho_{xx}^2$ relation can well describe the AHE in bulk Fe whisker measured at room temperature [15], it is evident that at low temperatures both the skew scattering and side jump are important and thus cannot be neglected when comparing with the Karplus-Luttinger intrinsic term; e.g., in the 6.5 nm film case at 5 K, the skew scattering $\rho_{\mathrm{sk}} = \alpha\rho_{xx0} = -4.2 \times 10^{-2}\ \mu\Omega\,\mathrm{cm}$, and the side jump $\rho_{\mathrm{sj}} = \beta\rho_{xx0}^2 = 8.9 \times 10^{-2}\ \mu\Omega\,\mathrm{cm}$, are significant compared with the Karplus-Luttinger intrinsic $\rho_{\mathrm{int}} = -\sigma_{\mathrm{int}}\rho_{xx0}^2 = 1.4 \times 10^{-1}\ \mu\Omega\,\mathrm{cm}$. Even in the bulklike 93 nm film case, the extrinsic contributions at 5 K are by no means small: $\rho_{\mathrm{sk}} = -1.4 \times 10^{-2}\ \mu\Omega\,\mathrm{cm}$, $\rho_{\mathrm{sj}} = 9.4 \times 10^{-3}\ \mu\Omega\,\mathrm{cm}$, and $\rho_{\mathrm{int}} = 1.5 \times 10^{-2}\ \mu\Omega\,\mathrm{cm}$. In addition, the negative sign of α indicates that the skew scattering contributes to the AHE in Fe in the opposite way as the side jump as well as the Karplus-Luttinger terms do. Therefore, in principle the former could exceed the latter and takes over at low temperature in purer samples with larger σ_{xx0} or smaller ρ_{xx0}. This offers an explanation to a long-standing striking puzzle that the AHE in Fe changes the sign simply as the temperature was lowered [15].

At last, our unified physical picture may encompass all aforementioned diverse possibilities outlined in the introduction. First, it is likely that type (a) corresponds to situations in which either the material dependent parameters α and β happen to be very small or the measurements were carried out at temperatures where $\rho_{xx0} \ll \rho_{xx}$. Second, type (b) actually belongs to a special case of Eq. (1) where the temperature was fixed very low (so $\rho_{xx} \approx \rho_{xx0}$), and the sample was ultrapure (so ρ_{xx0}^2 terms $\ll$ ρ_{xx0} term), so the equation becomes $\rho_{\mathrm{AH}} \approx \alpha\rho_{xx0}$. Third, we have reanalyzed the raw data of type (c) and found that the new scaling Eq. (1) can indeed better describe the experiments. Fourth, type (d) presumably corresponds to a nontrivial case of Eq. (1), where $b = -\sigma_{\mathrm{int}}$ itself is sensitive to temperature in the range of interest [22].

This work was supported by MSTC (No. 2009CB929203 and No. 2006CB921303), NSFC (No. 10834001), and SCST.

*Corresponding author.
xfjin@fudan.edu.cn

[1] E. H. Hall, Philos. Mag. **10**, 301 (1880).
[2] R. Karplus and J. M. Luttinger, Phys. Rev. **95**, 1154 (1954).
[3] J. Smit, Physica (Amsterdam) **24**, 39 (1958).
[4] J. M. Luttinger, Phys. Rev. **112**, 739 (1958).
[5] L. Berger, Phys. Rev. B **2**, 4559 (1970).
[6] *The Hall Effect and Its Applications*, edited by C. L. Chien and C. R. Westgate (Plenum, New York, 1980).
[7] J. Sinova *et al.*, Int. J. Mod. Phys. B **18**, 1083 (2004).
[8] N. Nagaosa, J. Phys. Soc. Jpn. **75**, 042001 (2006).
[9] N. A. Sinitsyn, J. Phys. Condens. Matter **20**, 023201 (2008).
[10] G. Sundaram *et al.*, Phys. Rev. B **59**, 14 915 (1999).
[11] T. Jungwirth *et al.*, Phys. Rev. Lett. **88**, 207208 (2002).
[12] M. Onoda *et al.*, J. Phys. Soc. Jpn. **71**, 19 (2002).
[13] J. Ye *et al.*, Phys. Rev. Lett. **83**, 3737 (1999).
[14] W. Jellinghaus *et al.*, Ann. Phys. (Leipzig) **462**, 189 (1961).
[15] P. N. Dheer, Phys. Rev. **156**, 637 (1967).
[16] W. L. Lee *et al.*, Science **303**, 1647 (2004).
[17] Y. Pu *et al.*, Phys. Rev. Lett. **101**, 117208 (2008).
[18] A. Fert *et al.*, Phys. Rev. Lett. **28**, 303 (1972).
[19] C. G. Zeng *et al.*, Phys. Rev. Lett. **96**, 037204 (2006).
[20] J. Kotzler *et al.*, Phys. Rev. B **72**, 060412 (2005).
[21] J. Lavine, Phys. Rev. **123**, 1273 (1961).
[22] Z. Fang *et al.*, Science **302**, 92 (2003).
[23] Y. Yao *et al.*, Phys. Rev. Lett. **92**, 037204 (2004).
[24] T. Miyasato *et al.*, Phys. Rev. Lett. **99**, 086602 (2007).
[25] N. Nagaosa *et al.*, arXiv:0904.4154.
[26] C. S. Tian *et al.*, Phys. Rev. Lett. **94**, 137210 (2005).
[27] L. F. Yin *et al.*, Phys. Rev. Lett. **97**, 067203 (2006).
[28] A. Crepieux *et al.*, Phys. Rev. B **64**, 014416 (2001).